Physica B 713 (2025) 417289

Contents lists available at ScienceDirect

Physica B: Condensed Matter

journal homepage: www.elsevier.com/locate/physb

Nonlinear lattice parameter–concentration relationship and its role in microstructural evolution of alloys

Jeonghwan Lee [a], Yulan Li [b], Shenyang Hu [b], Kunok Chang [a,*]

[a] Department of Nuclear Engineering, Kyung Hee University, Yong-in city, Korea
[b] Pacific Northwest National Laboratory, Richland, WA 99352, USA

ARTICLE INFO

Keywords:
Phase-field method
Non-linear elastic interaction
Microstructural evolution

ABSTRACT

Elastic interactions are a key driving force in microstructural evolution. While conventional phase-field models typically employ Vegard's law — assuming a linear dependence of lattice parameters on solute concentration — this approximation breaks down in concentrated alloys, where the relationship becomes inherently nonlinear. In this work, we develop an advanced phase-field model that explicitly incorporates nonlinear elastic interactions by capturing the nonlinear dependence of lattice parameters on concentration. This enhanced formulation reveals that such nonlinearities can substantially alter the equilibrium concentration profiles, leading to more accurate predictions of microstructural behavior.

1. Introduction

The elastic interactions in materials are important because they influence the microstructural evolution and affect morphology, which determines the mechanical performance of the material [1,2]. Therefore, understanding elastic interaction is necessary to predict the behaviors of the system that affect the structural integrity in materials.

To understand the elastic interaction in materials, Cahn and Larche proposed an analytical model for coherent equilibrium and analyzed the elastic effect on phase equilibria in a binary alloy [3]. They described analytic solutions through free energy minimization and showed the Williams point that a two-phase region does not exist due to the elastic interaction. Lee et al. [4] extended the elastic interaction theory by applying concentration-dependent misfit strain to the Cahn–Larche analysis.

However, previous studies have been limited to linear elastic interaction based on Vegard's law [5], which assumes that the lattice parameter changes linearly with concentration [6–8]. In real binary solution materials, the concentration and the lattice parameter are not always a linear correlation [9,10]. To explain the nonlinear relationship between the lattice parameter and the concentration, the bowing parameter was introduced by Fournet [11].

To investigate the influence of elastic interactions on the bowing parameter and microstructural evolution, we conducted phase-field simulations that capture both concentration and morphological changes across the entire system. While most phase-field models for phase transformations in binary alloys adopt Vegard's law — assuming a linear relationship between concentration and lattice parameter — we introduce a model that incorporates a nonlinear concentration–lattice parameter correlation. This advanced formulation is implemented using the MOOSE (Multiphysics Object Oriented Simulation Environment) framework [12], enabling a more realistic representation of elastic effects in concentrated alloy systems.

2. Phase-field methods with non-linear lattice parameter

2.1. Phase-field modeling using the Cahn–Hilliard equation

To investigate the effect of elastic interaction, we describe the evolution of the concentration field using the Cahn–Hilliard equation [13,14].

$$\frac{\partial c(\mathbf{r},t)}{\partial t} = M\nabla^2\left[\frac{\delta F(\mathbf{r},t)}{\delta c(\mathbf{r},t)}\right] \tag{1}$$

where $c(\mathbf{r},t)$ is the concentration, M is chemical mobility, and $F(\mathbf{r},t)$ is the total free energy of the system given by:

$$F(\mathbf{r},t) = \int_V \left[\frac{1}{V_m}\left(f(c(\mathbf{r},t)) + \frac{1}{2}\kappa(\nabla c(\mathbf{r},t))^2\right) + f_{El}(c(\mathbf{r},t))\right] dV \tag{2}$$

where $f(c(\mathbf{r},t))$ is the local free energy of the binary solution, κ is the interfacial energy coefficient, V_m is the molar volume and $f_{El}(c(\mathbf{r},t))$ is the elastic energy density related to lattice mismatch. We consider a regular solution model for local free energy.

* Corresponding author.
E-mail address: kunok.chang@khu.ac.kr (K. Chang).

https://doi.org/10.1016/j.physb.2025.417289
Received 20 January 2025; Received in revised form 16 April 2025; Accepted 21 April 2025
Available online 8 May 2025

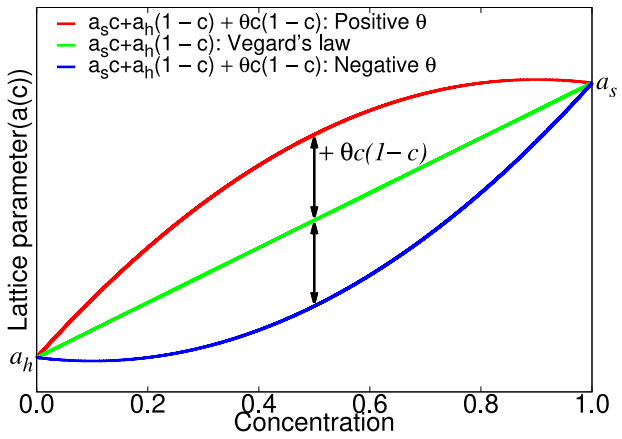

Fig. 1. The relationship between concentration and lattice parameter for varying bowing parameters.

$$f(c(\mathbf{r},t)) = \mu_s^{\circ} c + \mu_h^{\circ}(1-c) + RT[c\ln(c) + (1-c)\ln(1-c)] + \Omega c(1-c) \tag{3}$$

where μ_s° and μ_h° are free energies for solute and host atoms at reference state, R is the gas constant, T is the system's absolute temperature, and Ω is the interaction parameter between solute and host atoms.

2.2. The nonlinear relationship between concentration and lattice parameter

The elastic energy density($f_{El}(c(\mathbf{r},t))$) is directly affected by lattice distortions. Therefore, understanding how the lattice parameter varies with concentration is crucial. In the binary system, the lattice parameter($a(c)$) of a solid solution is determined by the lattice parameters of the pure solute(a_s) and host(a_h) atoms, as well as the concentration. In 1921, Vegard proposed an equation($a(c) = ca_s + (1-c)a_h$) to predict the lattice parameter of a binary solid solution by assuming a linear relationship between the lattice parameter of the system and the concentration. However, as in previous studies, the lattice parameter of metallic solid solutions often deviates from Vegard's law [10]. To explain the non-linearity between the lattice parameter and the concentration, Fournet [11] proposed Eq. (4) using the bowing parameter(θ).

$$a(c) = ca_s + (1-c)a_h + \theta c(1-c) \tag{4}$$

when θ is zero, the lattice parameter and concentration follow a linear relationship consistent with Vegard's law. For positive θ, the lattice parameter deviates positively from the linear relationship, while negative θ leads to a negative deviation, as shown in Fig. 1. Accordingly, the bowing parameter (θ) directly determines the extent of deviation from Vegard's law.

2.3. Eigenstrain for nonlinear lattice parameter

The eigenstrain concept introduced by Toshio Mura [15] is used to represent inelastic deformations, such as plastic deformations and thermal expansion mismatch. According to recent studies on the coherency elastic energy arising from compositional inhomogeneity, as the concentration departs from the nominal concentration, the eigenstrain exhibits a corresponding increase given by:

$$\varepsilon_{ij}^{\circ}(c(\mathbf{r})) = \delta_{ij}\varepsilon_0(c(\mathbf{r}))(c(\mathbf{r}) - c_0) \tag{5}$$

where $\varepsilon_{ij}^{\circ}(c(\mathbf{r}))$ is the eigenstrain for compositional inhomogeneity, δ_{ij} is the Kronecker delta function, and ε_0 is the lattice mismatch-related lattice expansion coefficient, which can be expressed as follows:

$$\varepsilon_0(c(\mathbf{r})) = \frac{1}{a_0}\frac{da(c(\mathbf{r}))}{dc(\mathbf{r})} \tag{6}$$

where a_0 is the lattice parameter at nominal concentration(c_0). In previous studies, where the lattice parameter is treated as a function of only the host atom, solute atom, and concentration, the lattice expansion coefficient is determined as a constant($\varepsilon_0 = \frac{a_s - a_h}{a_0}$). However, when the bowing parameter is considered, the lattice expansion coefficient becomes a linear function of concentration, described in Eq. (7).

$$\varepsilon_0(c(\mathbf{r})) = \frac{a_s - a_h}{a_0} + \frac{\theta(1-2c)}{a_0} \tag{7}$$

Therefore, the incorporation of the bowing parameter into the lattice expansion coefficient provides a more comprehensive representation of compositional inhomogeneity effects in real metallic binary solid solutions.

2.4. The nonlinear lattice parameter with second-order Taylor expansion

To analyze the effects of Vegard's law and the bowing parameter, respectively, we separate the lattice parameter into linear and nonlinear terms using a second-order Taylor expansion. Therefore, the lattice parameter is given as follows:

$$a(c) \approx a^T(c) = a(c)|_{c=c_0} + a'(c)|_{c=c_0}(c-c_0) + \frac{1}{2!}a''(c)|_{c=c_0}(c-c_0)^2 \tag{8}$$

where $a^T(c)$ is the lattice parameter expanded using a second-order Taylor expansion. In Eq. (8), $a(c)|_{c=c_0}$, represents the lattice parameter at the nominal concentration(c_0). The parameters $a'(c)|_{c=c_0}$ and $a''(c)|_{c=c_0}$ denote the first and second derivatives of the lattice parameter with respect to the nominal concentration(c_0).

By substituting the Taylor-expanded lattice parameter($a^T(c)$) into the definition of the lattice expansion coefficient, $\varepsilon_0(c(\mathbf{r}))$), the relationship between the lattice expansion coefficient and concentration can be derived, as shown in Eq. (9).

$$\varepsilon_0(c(\mathbf{r})) \approx \frac{1}{a_0}\frac{da^T(c(\mathbf{r}))}{dc(\mathbf{r})} = \underbrace{\frac{a_s - a_h}{a_0} + \frac{\theta(1-2c_0)}{a_0}}_{\varepsilon_0{}^{(I)}} - \underbrace{\frac{2\theta}{a_0}}_{\varepsilon_0{}^{(II)}}(c(\mathbf{r}) - c_0) \tag{9}$$

The first term in Eq. (9), $\frac{a_s - a_h}{a_0}$, represents the linear contribution to the lattice expansion coefficient, consistent with Vegard's law, which assumes a direct proportional relationship between the lattice parameter and solute concentration. On the other hand, the terms $\frac{\theta(1-2c_0)}{a_0} - \frac{2\theta}{a_0}(c(\mathbf{r}) - c_0)$ represent deviations from Vegard's law introduced by the bowing parameter (θ), reflecting the non-linear relationship between the lattice parameter and the concentration.

In Eq. (9), $\varepsilon_0{}^{(I)}$ and $\varepsilon_0{}^{(II)}$ denote the lattice expansion coefficients related to the linear and non-linear contributions, respectively. When the bowing parameter(θ) is zero, the lattice parameter becomes linearly proportional to the concentration, reducing the eigenstrain to the same form as in previous studies [6,7]. Therefore, accounting for the non-linear relationship between the lattice parameter and the concentration, the eigenstrain is expressed as:

$$\varepsilon_{ij}^{\circ}(c(\mathbf{r})) = \delta_{ij}\{\varepsilon_0{}^{(I)} + \varepsilon_0{}^{(II)}(c(\mathbf{r}) - c_0)\}(c(\mathbf{r}) - c_0) \tag{10}$$

2.5. Elastic energy contribution to total free energy

Elastic interaction plays a central role in determining the total free energy of materials, particularly in systems where mechanical deformation interacts with phase transformations and microstructural evolution [2]. Therefore, it is crucial to understand the impact of elastic energy on the system.

To calculate the elastic energy density, we apply the Khachaturyan's strain interpolation scheme (KHS) [16], which interpolates the stiffness tensor and the misfit strain to create a global representation of the system. The elastic energy density is expressed as:

$$f_{El}(c(\mathbf{r})) = \frac{1}{2}C_{ijkl}^{KHS}(c)\varepsilon_{ij}^{el}(\mathbf{r})\varepsilon_{kl}^{el}(\mathbf{r}) \tag{11}$$

where $C_{ijkl}^{KHS}(c)$ is the interpolated stiffness tensor defined by:

$$C_{ijkl}^{KHS}(c(\mathbf{r})) = C_{ijkl}^{solute}c(\mathbf{r}) + C_{ijkl}^{host}(1 - c(\mathbf{r})) \tag{12}$$

and $\varepsilon_{ij}(\mathbf{r})$ is the total strain, given as:

$$\varepsilon_{ij}(\mathbf{r}) = \varepsilon_{ij}^{hom} + \varepsilon_{ij}^{het}(\mathbf{r}) \tag{13}$$

where ε_{ij}^{hom} denotes the homogeneous strain, representing the macroscopic deformation of the system's shape. The homogeneous strain can be expressed as:

$$\varepsilon_{ij}^{hom} = \int_V \delta\varepsilon_{ij}(\mathbf{r})dV = 0 \tag{14}$$

On the other hand, $\varepsilon_{ij}^{het}(\mathbf{r})$ represents the heterogeneous strain, which is determined by the displacement fields. The heterogeneous strain can be described as:

$$\varepsilon_{ij}^{het}(\mathbf{r}) = \frac{1}{2}\left(\frac{\partial\mu_i}{\partial r_j} + \frac{\partial\mu_j}{\partial r_i}\right) \tag{15}$$

where μ_j represents the displacement field ith component at position r. Therefore, elastic energy density in an elastically inhomogeneous system is given by:

$$F_{El} = \frac{1}{2}C_{ijkl}^{KHS}(\varepsilon_{ij}(\mathbf{r}) - \varepsilon_{ij}^{0}(\mathbf{r}))(\varepsilon_{kl}(\mathbf{r}) - \varepsilon_{kl}^{0}(\mathbf{r})) \tag{16}$$

To maintain the mechanical equilibrium, the system must satisfy:

$$\nabla \cdot \sigma_{ij}(\mathbf{r}) = 0 \tag{17}$$

where $\sigma_{ij}(\mathbf{r})(= C_{ijkl}^{KHS}\varepsilon_{ij}^{el})$ is the local stress field.

2.6. Computational details

Our simulations employ non-dimensional values to enhance the computational efficiency. The non-dimensional total free energy, $F^*(\mathbf{r},t)$, is expressed as:

$$F^*(\mathbf{r},t) = \int_V \left[f^*(c(\mathbf{r},t)) + \frac{1}{2}\kappa^*(\nabla c(\mathbf{r},t))^2 + f_{El}^*(c(\mathbf{r},t))\right]dV \tag{18}$$

where $f^*(c(\mathbf{r},t)) = f(c(\mathbf{r},t))/(RT)$, non-dimensional interfacial energy coefficient is $\kappa^* = \frac{1}{6}\Omega/(RT)$ and $f_{El}^*(c(\mathbf{r},t)) = V_m f_{El}(c(\mathbf{r},t))/(RT)$.

To evaluate the microstructure evolution in the real metallic system, we considered properties in the Fe–Cr system at 673.15 K, a temperature at which the α and α' phases clearly separate, causing the well known 475 °C embrittlement in Fe–Cr system [17–19]. The interaction parameter of Fe–Cr system is $\Omega = (20500 - 9.68 \times T)$ J/mol in Eq. (3). The molar volume is $V_m = 1.4 \times 10^{-5}$ m^3/mol. The elastic constants in the Fe–Cr system are $C_{11}^{\mathrm{Fe}} = 205$ GPa, $C_{12}^{\mathrm{Fe}} = 129$ GPa, $C_{44}^{\mathrm{Fe}} = 109$ GPa at 672 K and $C_{11}^{\mathrm{Cr}} = 365$ GPa, $C_{12}^{\mathrm{Cr}} = 115$ GPa, and $C_{44}^{\mathrm{Cr}} = 96$ GPa at 650 K[20,21].

We consider five cases of bowing parameters with the corresponding lattice parameter variations shown in Fig. 2. To investigate the effects of the bowing parameter (θ), appropriate values were selected to represent varying deviations from Vegard's law. Five cases, including positive values (cases 4, 5), negative values (cases 1, 2), and zero (case 3) bowing parameter values, were analyzed to explore their impacts on the lattice parameter profiles, as shown in Fig. 2.

The initial condition assumes the presence of an inclusion within the matrix, where the concentrations are set to 14.5 at% in the matrix and 85.5 at% in the inclusion, as shown in Fig. 3. The simulation cell size is $200\Delta x \times 200\Delta y$. The inclusion has a radius of $r = 55.7\Delta x$, with the nominal concentration in all cases is 31.7 at%. Moreover, periodic boundary conditions for concentration and Dirichlet boundary conditions for displacement are applied along both Cartesian axes.

3. Simulation results

We observed equilibrium concentration, precipitate size, and precipitate morphology in the five cases with different bowing parameters.

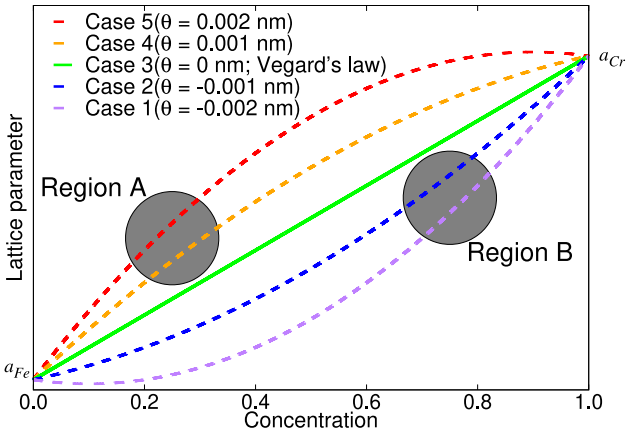

Fig. 2. The lattice parameter corresponding to concentration for each case. Region A corresponds to the area with significant lattice parameter changes at low concentrations, whereas Region B indicates significant changes at high concentrations.

As shown in Fig. 4, the shape evolution of an isolated particle was determined by solving the Cahn–Hilliard diffusion equation, incorporating the effects of elastic stress. Without elastic stress in the system (Fig. 4(a)), the equilibrium shape formed as an isotropic circle. However, when elastic interaction was included (Fig. 4(b)–(f)), the equilibrium shape transitioned to a cubic morphology with rounded corners, driven by the anisotropic distribution of elastic strain energy.

The particle size was analyzed for five simulation cases to evaluate the influence of the bowing parameter (θ) and elastic interaction on the equilibrium morphology. In Fig. 4 and Table 1, the particle size decreased with an increase in the bowing parameter. Moreover, the coherent equilibrium concentration within the inclusion was lower than the incoherent equilibrium concentration, driven by the elastic strain energy. As observed in region B of Fig. 2, the elastic driving force ($\frac{\partial F(\mathbf{r},t)}{\partial c}$) decreased with an increase in the bowing parameter (as slope decreases). Consequently, the coherent equilibrium concentration approached the incoherent equilibrium concentration due to the reduced influence of the elastic strain energy.

The total concentration of the system must be conserved. Considering elastic interaction, the equilibrium concentration within the inclusion increases as the bowing parameter increases, because of the contribution of elastic energy to the total free energy. Therefore, the particle size decreases as the bowing parameter increases, as shown in Table 1

As shown in Fig. 5, when the elastic interaction did not contribute to the total free energy, the concentration within the inclusion was 85.5 at%, while the matrix concentration was 14.5 at%. In case 3, where a linear relationship between lattice parameter and concentration, the symmetric reduction in the miscibility gap shifted towards each other under the influence of elastic interaction.

For a negative bowing parameter (case 1 and case 2), the concentration change in inclusion was more pronounced than that in the matrix. However, when the bowing parameter was positive (case 4 and case 5), the matrix's concentration change was more significant than that in the inclusion. Moreover, as the absolute value of the bowing parameter($|\theta|$) increased, the equilibrium concentration change induced by the elastic interaction became more pronounced. Therefore, the negative bowing parameter led to a high equilibrium dominant miscibility gap reduction, whereas the positive bowing parameter caused a low equilibrium dominant miscibility gap reduction.

The asymmetric reduction in the miscibility gap was driven by the slope variations of the lattice parameter, as shown in Fig. 1. In case 1 and case 2, the dominant change occurred at higher concentrations (Region B), where the slope increased significantly. In contrast, case 4 and

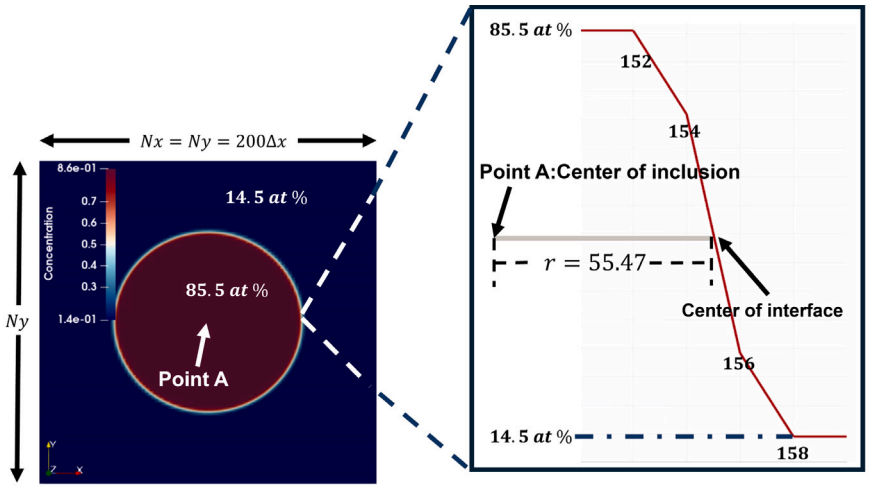

Fig. 3. Simulation initial condition illustrating an inclusion within the matrix. The equilibrium concentrations are set to 14.5 at% in the matrix and 85.5 at% in the inclusion.

Table 1
The bowing parameters (θ), particle size, and concentration in the inclusion for five simulation cases.

Case	Bowing parameter (θ)	Particle size	Concentration in the inclusion
Without elastic interaction		$4769.97\Delta x\Delta y$	0.855
1	−0.002 nm	$6310.52\Delta x\Delta y$	0.487
2	−0.001 nm	$5078.08\Delta x\Delta y$	0.577
3	0 nm	$3977.42\Delta x\Delta y$	0.773
4	0.001 nm	$3319.36\Delta x\Delta y$	0.852
5	0.002 nm	$2353.84\Delta x\Delta y$	0.832

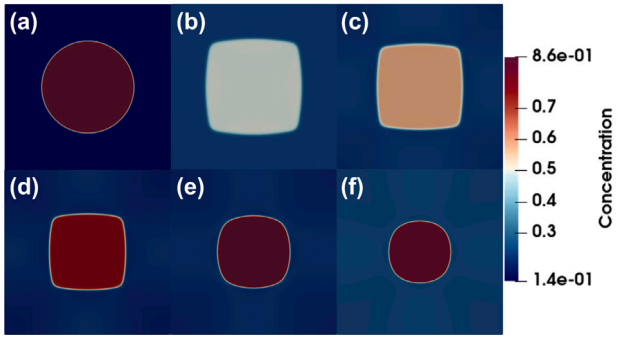

Fig. 4. The concentration field for the five cases with different bowing parameters at equilibrium state. (a) represents the case without elastic energy density, (b) corresponds to case 1, (c) to case 2, (d) to case 3, (e) to case 4, and (f) to case 5.

case 5 showed significant deviations at lower concentrations(Region A) due to the steeper slope at low concentrations.

As θ increased from case 1 to case 4, the concentration in the inclusion increased. In case 4, the inclusion concentration became almost identical to the upper limit, which was the concentration observed without elastic interaction. On the other hand, the concentration in the matrix decreased as θ increased from case 1 to case 3. From case 3 to case 5, the concentration increased as θ increases. When comparing case 4 and case 5, the increase in matrix concentration due to the increase in θ became more pronounced, which appeared to have caused a slight decrease in inclusion concentration.

To validate the simulation results, including equilibrium concentrations and reduction of the asymmetric miscibility gap, analytical solutions were derived and compared with the phase-field simulation results to ensure consistency. We considered a binary regular solution model described by a local incoherent free energy density ($f_{Local}(c)$) and an elastic energy density ($f_{El}(\varepsilon_{ij}, c)$). Therefore, the free energy of the system is $F = f_{Local}(c) + f_{El}(\varepsilon_{ij}, c)$ without interface.

$$f_{Local}(c) = RT(c\ln c + (1-c)\ln(1-c)) + \Omega_0 c(1-c) \tag{19}$$

$$f_{El}(\varepsilon_{ij}, c) = \frac{1}{2}C_{ijkl}\{\varepsilon_{ij} - \delta_{ij}\varepsilon_0(c-c_0)\}\{\varepsilon_{kl} - \delta_{kl}\varepsilon_0(c-c_0)\} \tag{20}$$

where Ω_0 is the interaction parameter in binary alloy independent temperature in (19). We assume that $\varepsilon_{ij} = 0$, and consider $\varepsilon^0_{ij} = \frac{a_s - a_h}{a_0} + \frac{\theta(1-2c)}{a_0}$ in the Eq. (7). The partial free energies are given by:

$$\frac{\partial f_{Local}(c)}{\partial c} = RT\ln\left(\frac{c}{1-c}\right) + \Omega_0(1-2c) \tag{21}$$

$$\left.\frac{\partial f_{El}(c)}{\partial c}\right|_{\varepsilon_{ij}} = -\left\{\varepsilon_0 - \frac{2\theta}{a_0}(c-c_0)\right\}\sigma_{jj} \tag{22}$$

Using Eqs. (21) and (22), we computed the phase boundary (solvus curve) that defines the solubility limit in the phase diagram at a given normalized temperature RT/Ω, and showed that they vary significantly with the bowing parameter (θ), under assumption $\varepsilon_{ij} = 0$, as shown in Fig. 6. Specifically, elastic interactions induced by the bowing parameter cause asymmetric shifts in equilibrium concentrations, leading to more pronounced changes on the inclusion side (higher concentration) than on the matrix side (lower concentration). Therefore, these analytical predictions show qualitative agreement with our simulation results.

4. Conclusions

This study demonstrates that the bowing parameter, which quantifies the nonlinear relationship between the lattice parameter and concentration, plays a critical role in creating an asymmetric reduction in equilibrium concentrations between the matrix and the precipitate. As the bowing parameter increases, the equilibrium concentration within the inclusion approaches the incoherent equilibrium concentration as a result of the redistribution of elastic strain energy. An increase in the bowing parameter also leads to a reduction in particle

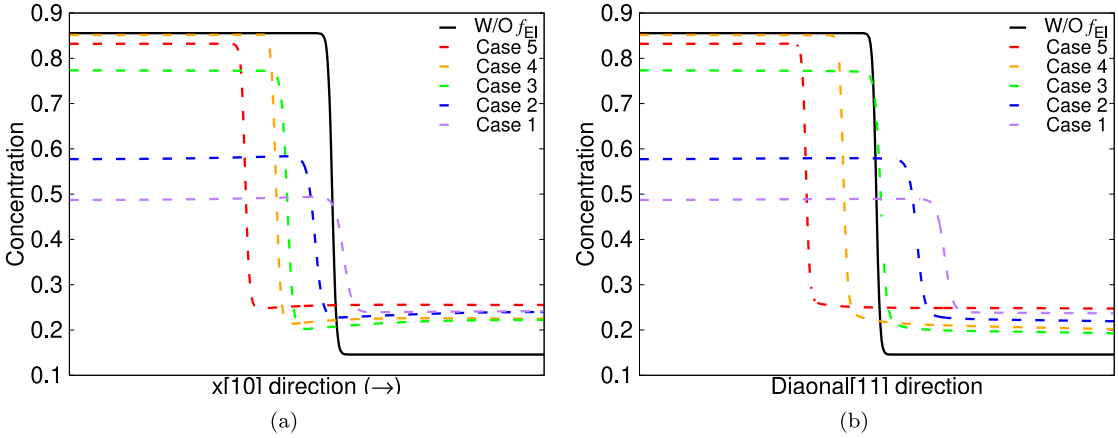

Fig. 5. Concentration profiles were obtained using the phase-field method for various cases. The profiles are shown from the center of the inclusion to the matrix boundary along (a) [10]- and (b) [11]-directions.

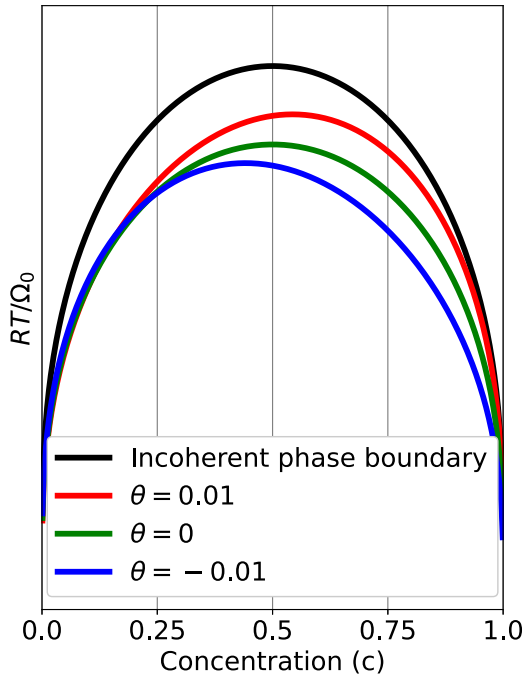

Fig. 6. Phase diagram showing the effect of elastic interactions on phase boundaries. The black line corresponds to the incoherent case (no elastic interaction($f_{EI} = 0$)). Colored lines represent coherent cases corresponding to different θ values: red($\theta = 0.01$), green($\theta = 0$), and blue($\theta = -0.01$).

size, reflecting the interplay between the elastic interaction and the conservation of total concentration.

Moreover, a negative bowing parameter results in a more significant concentration change in the precipitate compared to the matrix, while a positive bowing parameter shifts the dominant change to the matrix. In particular, the magnitude of the bowing parameter amplifies the asymmetry in equilibrium concentration changes between the matrix and the precipitate.

CRediT authorship contribution statement

Jeonghwan Lee: Writing – original draft, Methodology, Investigation, Data curation. **Yulan Li:** Writing – review & editing, Conceptualization. **Shenyang Hu:** Writing – review & editing. **Kunok Chang:** Writing – review & editing, Validation, Project administration, Funding acquisition, Conceptualization.

Declaration of competing interest

The authors declare the following financial interests/personal relationships which may be considered as potential competing interests: Kunok Chang reports financial support was provided by Korea Institute of Energy Technology Evaluation and Planning. If there are other authors, they declare that they have no known competing financial interests or personal relationships that could have appeared to influence the work reported in this paper.

Acknowledgments

This work was supported by the Korea Institute of Energy Technology Evaluation and Planning, South Korea (KETEP) and the Ministry of Trade, Industry & Energy(MOTIE) of the Republic of Korea (No. 20214000000790). This work was also supported by the National Research Foundation of Korea(NRF) grant funded by the Korea government(MSIP) (RS-2023-00229215)

Data availability

Data will be made available on request.

References

[1] J.R. Barber, Elasticity, Springer, 2002.
[2] L.-Q. Chen, Phase-field models for microstructure evolution, Annu. Rev. Mater. Res. 32 (1) (2002) 113–140.
[3] J. Cahn, F. Larché, A simple model for coherent equilibrium, Acta Metall. 32 (11) (1984) 1915–1923.
[4] J.K. Lee, W. Tao, Coherent phase equilibria: effect of composition-dependent elastic strain, Acta Met. et Mater. 42 (2) (1994) 569–577.
[5] L. Vegard, Die konstitution der mischkristalle und die raumfüllung der atome, Z. Für Phys. 5 (1) (1921) 17–26.
[6] S. Hu, L. Chen, Solute segregation and coherent nucleation and growth near a dislocation—a phase-field model integrating defect and phase microstructures, Acta Mater. 49 (3) (2001) 463–472.
[7] T.W. Heo, S. Bhattacharyya, L.-Q. Chen, A phase field study of strain energy effects on solute–grain boundary interactions, Acta Mater. 59 (20) (2011) 7800–7815.
[8] M. Asle Zaeem, H. El Kadiri, S.D. Mesarovic, M.F. Horstemeyer, P.T. Wang, Effect of the compositional strain on the diffusive interface thickness and on the phase transformation in a phase-field model for binary alloys, J. Phase Equilibria Diffus. 32 (2011) 302–308.
[9] V. Lubarda, On the effective lattice parameter of binary alloys, Mech. Mater. 35 (1–2) (2003) 53–68.
[10] O. Abdullah, Modeling the lattice parameters of solid solution alloys, Anchor Academic Publishing, 2017.
[11] G. Fournet, Étude de la loi de vegard, J. Phys. Radium 14 (6) (1953) 374–380.

[12] D. Gaston, C. Newman, G. Hansen, D. Lebrun-Grandie, MOOSE: A parallel computational framework for coupled systems of nonlinear equations, Nucl. Eng. Des. 239 (10) (2009) 1768–1778.
[13] J.W. Cahn, J.E. Hilliard, Free energy of a nonuniform system. I. Interfacial free energy, J. Chem. Phys. 28 (2) (1958) 258–267.
[14] J.W. Cahn, On spinodal decomposition, Acta Metall. 9 (9) (1961) 795–801.
[15] T. Mura, Micromechanics of defects in solids, Springer Science & Business Media, 2013.
[16] A.G. Khachaturyan, Theory of structural transformations in solids, Courier Corporation, 2013.
[17] H. Solomon, L.M. Levinson, Mössbauer effect study of '475 c embrittlement'of duplex and ferritic stainless steels, Acta Metall. 26 (3) (1978) 429–442.
[18] P. Grobner, The 885 f (475 c) embrittlement of ferritic stainless steels, Met. Trans. 4 (1973) 251–260.
[19] D. Chandra, L. Schwartz, Mössbauer effect study of the 475‡c decomposition of fe-cr, Met. Trans. 2 (2) (1971) 511–519.
[20] D. Dever, Temperature dependence of the elastic constants in α-iron single crystals: relationship to spin order and diffusion anomalies, J. Appl. Phys. 43 (8) (1972) 3293–3301.
[21] K. Katahara, M. Nimalendran, M. Manghnani, E. Fisher, Elastic moduli of paramagnetic chromium and ti-V-Cr alloys, J. Phys. F: Met. Phys. 9 (11) (1979) 2167.